



New Aggregation-Induced Delayed Fluorescence Luminogens With Through-Space Charge Transfer for Efficient Non-doped OLEDs

Panpan Zhang¹, Jiajie Zeng¹, Jingjing Guo¹, Shijie Zhen¹, Biao Xiao², Zhiming Wang¹, Zujin Zhao^{1*} and Ben Zhong Tang^{1,3*}

¹ State Key Laboratory of Luminescent Materials and Devices, Center for Aggregation-Induced Emission, South China University of Technology, Guangzhou, China, ² Key Laboratory of Optoelectronic Chemical Materials and Devices, School of Chemical and Environmental Engineering, Jiangnan University, Ministry of Education, Wuhan, China, ³ Department of Chemistry, Hong Kong Branch of Chinese National Engineering Research Center for Tissue Restoration and Reconstruction, The Hong Kong University of Science and Technology, Hong Kong, China

OPEN ACCESS

Edited by:

Lian Duan,
Tsinghua University, China

Reviewed by:

CaiJun Zheng,
University of Electronic Science and
Technology of China, China
Christopher Pigge,
The University of Iowa, United States

*Correspondence:

Zujin Zhao
mszjzhao@scut.edu.cn
Ben Zhong Tang
tangbenz@ust.hk

Specialty section:

This article was submitted to
Organic Chemistry,
a section of the journal
Frontiers in Chemistry

Received: 18 January 2019

Accepted: 15 March 2019

Published: 05 April 2019

Citation:

Zhang P, Zeng J, Guo J, Zhen S,
Xiao B, Wang Z, Zhao Z and Tang BZ
(2019) New Aggregation-Induced
Delayed Fluorescence Luminogens
With Through-Space Charge Transfer
for Efficient Non-doped OLEDs.
Front. Chem. 7:199.
doi: 10.3389/fchem.2019.00199

In this work, two tailor-made luminogens comprising of electron donors (acridine and phenoxazine) and acceptor (triazine) bridged by the through-space conjugated hexaphenylbenzene (HPB) are synthesized and characterized. Their thermal stability, electrochemical behaviors, crystal, and electronic structures, and photophysical properties are systematically investigated. The crystal and electronic structures reveal that the peripheral phenyls in HPB are closely aligned in a propeller-like fashion, rendering efficient through-space charge transfer between donor and electron moieties. These molecules display weak fluorescence with negligible delayed component in solutions but strong fluorescence with greatly increased delayed component upon aggregate formation, namely aggregation-induced delayed fluorescence (AIDF). Their neat films exhibit high photoluminescence quantum yields (PLQY), and prominent delayed fluorescence. The non-doped organic light-emitting diodes (OLEDs) based on these new luminogens exhibit excellent performance with maximum external quantum efficiency of 12.7% and very small efficiency roll-off of 2.7% at 1,000 cd m⁻². Designing AIDF molecules with through-space charge transfer could be a promising strategy to explore robust luminescent materials for efficient non-doped OLEDs.

Keywords: aggregation-induced delayed fluorescence, thermally activated delayed fluorescence, through-space charge transfer, organic light-emitting diodes, hexaphenylbenzene

INTRODUCTION

Organic light-emitting diodes (OLEDs) have been extensively studied owing to their excellent properties, such as flexibility, light weight, energy conservation, and so forth, and have gradually become a highly promising technology for flat panel display and white lighting. Organic electroluminescent materials are the foundation of OLEDs. The first-generation luminescent materials for OLEDs are fluorescent materials, such as tris(8-hydroxyquinolino)aluminum (Alq₃) (Tang and VanSlyke, 1987). But the efficiency of the device is greatly limited because only 25% singlet excitons are harvested for light emission in devices. The second-generation luminescent materials are phosphorescent materials that can achieve almost 100% exciton utilization via strong

spin orbit coupling of heavy metals such as platinum and iridium (Baldo et al., 1998; Adachi et al., 2001; Sasabe and Kido, 2013; Minaev et al., 2014). However, the scarcity and high price of noble metals greatly increase the device cost. So, the search for efficient and cheap luminescent materials still remains an urgent task. In response to these issues, several alternative strategies have been proposed, among which purely organic materials with thermally activated delayed fluorescence (TADF) have received the most interest (Endo et al., 2009; Gong et al., 2011; Wang et al., 2014; Zhang et al., 2014; Hirata et al., 2015; Seino et al., 2016). The OLEDs based on TADF emitters can extract light from both triplet and singlet excitons via spin-converting reverse intersystem crossing (RISC) under thermal activation, theoretically granting excellent internal quantum efficiencies (IQE) of up to 100% of the devices (Sun et al., 2014; Kaji et al., 2015; Lee et al., 2015a).

Generally, TADF emitters adopt highly twisted electron donor-acceptor (D-A) structures to realize small ΔE_{ST} , but the PLQY are often reduced, particularly in the aggregated state, which require doping technique in device fabrication. Recently, an interesting strategy to balance ΔE_{ST} and PLQY by through-space charge transfer effect has been proposed (Kawasumi et al., 2015; Rajamalli et al., 2016; Chen et al., 2017; Tsujimoto et al., 2017). For example, Wang et al. (Shao et al., 2017) took advantage of through-space charge transfer between D and A to realize blue TADF polymers with a non-conjugated polyethylene backbone. Spatial electronic coupling between D and A units results in small ΔE_{ST} (0.019 eV) and high PLQY (60%) in film. The resulting blue polymers exhibited good EL performance with a high EL efficiency of 12.1%. In these materials, D and A are physically separated but are spatially proximate. On one hand, the sufficient separation of highest occupied molecular orbital (HOMO) and lowest unoccupied molecular orbital (LUMO) is achieved, resulting in small ΔE_{ST} and thus delayed fluorescence. On the other hand, the electron clouds of D and A can interact with each other via a through-space manner to expedite the radiative transition rate, and enhanced PLQY can be expected.

It is well-known that most TADF emitters need complicated doping technique to suppress emission quenching and exciton annihilation (Tao et al., 2014; Furue et al., 2016). However, severe efficiency roll-off still happens as luminance increases, which impedes their large-scale commercial application (Cao et al., 2017). According to the recent studies, aggregation-induced delayed fluorescence (AIDF) materials provide an advisable strategy for solving this problem (Guo et al., 2017a, 2018a; Huang et al., 2017; Liu et al., 2018). Aggregation-induced delayed fluorescence (AIDF) luminogens are free of concentration quenching, and can exhibit strong delayed fluorescence upon aggregate formation. And the triplet excitons are rapidly converted to singlet excitons by RISC, inducing increased EL efficiency. Furthermore, AIDF luminogens present a highly twisted conformation, which can weaken intermolecular interactions and thus reduces short-range Dexter energy transfer. In consequence, non-doped OLEDs based on AIDF luminogens provide very small efficiency roll-off (Gan et al., 2016; Guo et al., 2017b).

Hexaphenylbenzene (HPB) derivatives have attracted intense research interest because of their fantastic geometry and wide application prospects (Waldvogel et al., 1999; Geng et al., 2001; Balzani et al., 2003; Tanaka et al., 2010; Lambert et al., 2012). HPB not only exhibits strong toroidal delocalization of π -electrons (Sun et al., 2005; Vij et al., 2016) but also has noteworthy aggregation-induced emission (AIE) property (Cho et al., 2006; Kanibolotsky et al., 2010). Integrating various D-A systems into HPB allows us to regulate molecular orbitals distribution, therefore adjust the ΔE_{ST} value and realize delayed fluorescence. Based on these considerations, herein, we develop two novel luminogens containing an electron D-A system built on HPB. The D and A moieties are positioned in close proximity so that electron clouds of D and A can communicate with each other through spatial interactions. The designed HPB-based molecules exhibit distinct AIDF property, and furnish efficient non-doped OLEDs with very small efficiency roll-off.

EXPERIMENTAL

Synthesis

2-(4-Ethynylphenyl)-4,6-diphenyl-1,3,5-triazine (**2**): Into a 250 mL two-necked round bottom flask was placed compound **1** (7.765 g, 20 mmol), trimethylsilylacetylene (5.653 mL, 40 mmol), Pd(PPh₃)₂Cl₂ (1.404 g, 2 mmol), copper iodide (0.761 g, 4 mmol), and PPh₃ (1.049 g, 4 mmol). The flask was evacuated under vacuum and flushed with dry nitrogen by three times and a mixed solvent system of tetrahydrofuran (THF) and triethylamine (100 mL, v/v = 1: 3) was injected. The reaction mixture was refluxed for 12 h. After cooling to room temperature, the mixture was poured into water and extracted with dichloromethane by three times. The combined organic layers were dried over anhydrous magnesium sulfate. After filtration and solvent evaporation, a mixture of the resulting crude product, KOH (2.0 g, 35.7 mmol) and K₂CO₃ (2.0 g, 14.5 mmol) were added into a mixed solvent system of methanol and THF (60 mL, v/v = 1: 1), and then stirred at room temperature for 12 h. The mixture was poured into water and extracted with dichloromethane by three times. The combined organic layers were dried over anhydrous magnesium sulfate. After filtration and solvent evaporation, the crude product was purified by silica-gel column chromatography (dichloromethane: petroleum ether, v/v = 1: 7). White solid of compound **2** was obtained in 65% yield. ¹H NMR (400 MHz, CDCl₃), δ (TMS, ppm): 8.8–8.73 (m, 6H), 7.70 (d, *J* = 8.4 Hz, 2H), 7.66–7.56 (m, 6H), 3.27 (s, 1H); ¹³C NMR (125 MHz, CDCl₃), δ (TMS, ppm): 171.90, 171.06, 136.63, 136.23, 132.78, 132.53, 129.14, 128.94, 128.83, 126.30, 83.55, 79.88. HRMS (C₂₃H₁₅N₃): *m/z* 334.1354 [M + H⁺, calcd 334.1344].

10-(4-((4-(4,6-Diphenyl-1,3,5-triazin-2-yl)phenyl)ethynyl)phenyl)-10-phenoxazine (**5a**): Into a 250 mL two-necked round bottom flask was placed compound **2** (3.331 g, 10 mmol), compound **3** (1.685 g, 5 mmol), Pd(PPh₃)₂Cl₂ (0.351 g, 0.5 mmol), copper iodide (0.190 g, 1 mmol), and PPh₃ (0.262 g, 1 mmol). The flask was evacuated under vacuum and flushed with dry nitrogen by three times and a mixed solvent system of THF and triethylamine (100 mL, v/v = 1: 3) was

injected. The reaction mixture was refluxed for 12 h. After cooling to room temperature, the mixture was poured into water and extracted with dichloromethane by three times. The combined organic layers were dried over anhydrous magnesium sulfate. After filtration and solvent evaporation, the crude product was purified by silica-gel column chromatography (dichloromethane: petroleum ether, v/v = 1: 10). Yellow solid of compound **5a** was obtained in 23% yield. ^1H NMR (500 MHz, CDCl_3), δ (TMS, ppm): 8.82–8.78 (m, 6H), 7.81 (d, J = 7.0 Hz, 2H), 7.76 (d, J = 8.4 Hz, 2H), 7.66–7.58 (m, 6H), 7.38 (d, J = 7.4 Hz, 2H), 6.73–6.59 (m, 6H), 5.97 (s, 2H); ^{13}C NMR (100 MHz, CDCl_3), δ (TMS, ppm): 171.90, 171.10, 146.31, 144.09, 136.35, 136.26, 134.56, 134.17, 132.79, 132.06, 131.21, 129.15, 129.08, 128.84, 127.15, 123.43, 121.73, 116.01, 115.72, 113.40, 91.23, 90.70. HRMS ($\text{C}_{41}\text{H}_{26}\text{N}_4\text{O}$): m/z 590.2086 [M^+ , calcd 590.2107].

10-(4-(4-(4,6-Diphenyl-1,3,5-triazin-2-yl)phenyl)ethynyl)phenyl-9,9-dimethyl-9,10-dihydroacridine (**5b**): The procedure was analogous to that described for **5a**. White solid of compound **5b** was obtained in 25% yield. ^1H NMR (500 MHz, CDCl_3), δ (TMS, ppm): 8.83–8.78 (m, 6H), 7.85 (d, J = 8.4 Hz, 2H), 7.78 (d, J = 8.6 Hz, 2H), 7.66–7.58 (m, 6H), 7.49–7.46 (m, 2H), 7.38 (d, J = 8.4 Hz, 2H), 7.02–6.98 (m, 2H), 6.97–6.93 (m, 2H), 6.31 (d, J = 8.0 Hz, 2H), 1.7 (s, 6H); ^{13}C NMR (125 MHz, CDCl_3), δ (TMS, ppm): 171.90, 171.12, 141.70, 140.80, 136.29, 136.28, 134.41, 132.78, 132.06, 131.71, 130.30, 129.15, 129.09, 128.84, 127.27, 126.56, 125.45, 123.11, 120.94, 114.17, 91.46, 90.54, 36.15, 31.37. HRMS ($\text{C}_{44}\text{H}_{32}\text{N}_4$): m/z 616.2616 [M^+ , calcd 616.2627].

10-(4''-(4,6-Diphenyl-1,3,5-triazin-2-yl)-3',4',5',6'-tetraphenyl-[1,1':2',1''-terphenyl]-4-yl)-10H-pheno-xazine (TRZ-HPB-PXZ): Into a 50 mL two-necked round bottom flask was placed a mixture of tetraphenylcyclopentadienone (0.922 g, 2.4 mmol) and compound **5a** (1.180 g, 2 mmol) and then diphenyl ether (15 mL) was added. The mixture was refluxed for 10 h and then cooled to room temperature. Ethanol was added into the mixture to precipitate the product, which was collected and washed with ethanol. Yellow solid of TRZ-HPB-PXZ was obtained in 56% yield. ^1H NMR (400 MHz, CDCl_3), δ (TMS, ppm): 8.74–8.69 (m, 4H), 8.47–8.42 (m, 2H), 7.62–7.57 (m, 2H), 7.56–7.51 (m, 4H), 7.15–7.12 (m, 2H), 7.11–7.07 (m, 2H), 6.96–6.87 (m, 20H), 6.84–6.80 (m, 2H), 6.52–6.48 (m, 2H), 6.43–6.30 (m, 4H), 5.48 (d, J = 7.8 Hz, 2H); ^{13}C NMR (125 MHz, CDCl_3), δ (TMS, ppm): 171.63, 171.27, 145.67, 144.85, 143.81, 143.79, 141.49, 141.47, 141.13, 140.95, 140.52, 140.40, 140.37, 140.36, 140.32, 140.18, 139.82, 139.72, 136.31, 134.19, 133.33, 132.59, 132.12, 131.63, 131.53, 131.52, 131.49, 129.04, 128.72, 127.53, 127.09, 126.91, 126.90, 126.87, 125.87, 125.66, 125.61, 125.57, 123.31, 115.81, 115.16, 113.20. HRMS ($\text{C}_{69}\text{H}_{46}\text{N}_4\text{O}$): m/z 946.3687 [M^+ , calcd 946.3672].

10-(4''-(4,6-Diphenyl-1,3,5-triazin-2-yl)-3',4',5',6'-tetraphenyl-[1,1':2',1''-terphenyl]-4-yl)-9,9-dimethyl-9,10-dihydroacridine (TRZ-HPB-DMAC): The procedure was analogous to that described as TRZ-HPB-PXZ. White solid of TRZ-HPB-DMAC was obtained in 60% yield. ^1H NMR (500 MHz, CDCl_3), δ (TMS, ppm): 8.74–8.71 (m, 4H), 8.48 (d, J = 8.2 Hz, 2H), 7.61–7.57 (m, 2H), 7.56–7.52 (m, 4H), 7.27 (s, 1H),

7.17 (d, J = 8.1 Hz, 2H), 7.12 (d, J = 8.0 Hz, 2H), 6.98–6.87 (m, 21H), 6.84–6.79 (m, 4H), 6.61–6.57 (m, 2H), 5.88–5.85 (m, 2H), 1.52 (s, 6H); ^{13}C NMR (125 MHz, CDCl_3), δ (TMS, ppm): 171.52, 171.19, 145.66, 141.05, 140.96, 140.80, 140.55, 140.48, 140.36, 140.32, 140.18, 140.14, 139.97, 139.66, 138.18, 136.24, 133.87, 133.22, 132.46, 132.09, 131.59, 131.47, 131.44, 131.42, 129.77, 129.61, 128.95, 128.62, 127.46, 126.98, 126.81, 126.79, 126.76, 126.30, 125.75, 125.58, 125.50, 125.44, 124.95, 120.19, 113.88, 35.84, 31.23. HRMS ($\text{C}_{72}\text{H}_{52}\text{N}_4$): m/z 972.4164 [M^+ , calcd 972.4192].

X-Ray Crystallography

Crystal data for TRZ-HPB-DMAC (CCDC 1885466): $\text{C}_{72}\text{H}_{52}\text{N}_4$, M_W = 973.17, monoclinic, C 2/c, a = 31.3912(15), b = 10.8163(6), c = 39.535(3) Å, β = 110.8700(10)°, V = 12542.9(13) Å³, Z = 8, D_c = 1.031 g cm⁻³, μ = 0.060 mm⁻¹ (MoK α , λ = 0.71073), $F(000)$ = 4096, T = 173(2) K, $2\theta_{\text{max}}$ = 25.242° (98.2%), 41548 measured reflections, 11317 independent reflections (R_{int} = 0.0914), GOF on F^2 = 1.076, R_1 = 0.1503, wR_2 = 0.1529 (all data), R_1 = 0.0684, wR_2 = 0.1296 [$I > 2\sigma(I)$], Δe 0.206 and -0.251 eÅ^{-3} .

OLED Fabrication and Characterization

Glass substrates pre-coated with a 95 nm thin layer of indium tin oxide (ITO) with a sheet resistance of 20 Ω per square were thoroughly cleaned for 10 min in ultrasonic bath of acetone, isopropyl alcohol, detergent, deionized water, and isopropyl alcohol and then treated with O₂ plasma for 5 min in sequence. Organic layers were deposited onto the ITO-coated substrates by high-vacuum ($< 5 \times 10^{-4}$ Pa) thermal evaporation. Deposition rates were controlled by independent quartz crystal oscillators, which were 1 ~ 2 Å s⁻¹ for organic materials, 0.1 Å s⁻¹ for LiF, and 6 Å s⁻¹ for Al, respectively. The emission area of the devices was 3 × 3 mm⁻² as shaped by the overlapping area of the anode and cathode. All the device characterization steps were carried out at room temperature under ambient laboratory conditions without encapsulation except spectrum collection process. EL spectra were taken by an optical analyzer, Photo Research PR705. Current density and luminance vs. driving voltage characteristics were measured by Keithley 2,420 and Konica Minolta chromameter CS-200, respectively. External quantum efficiencies were calculated by assuming that the devices were Lambertian light sources.

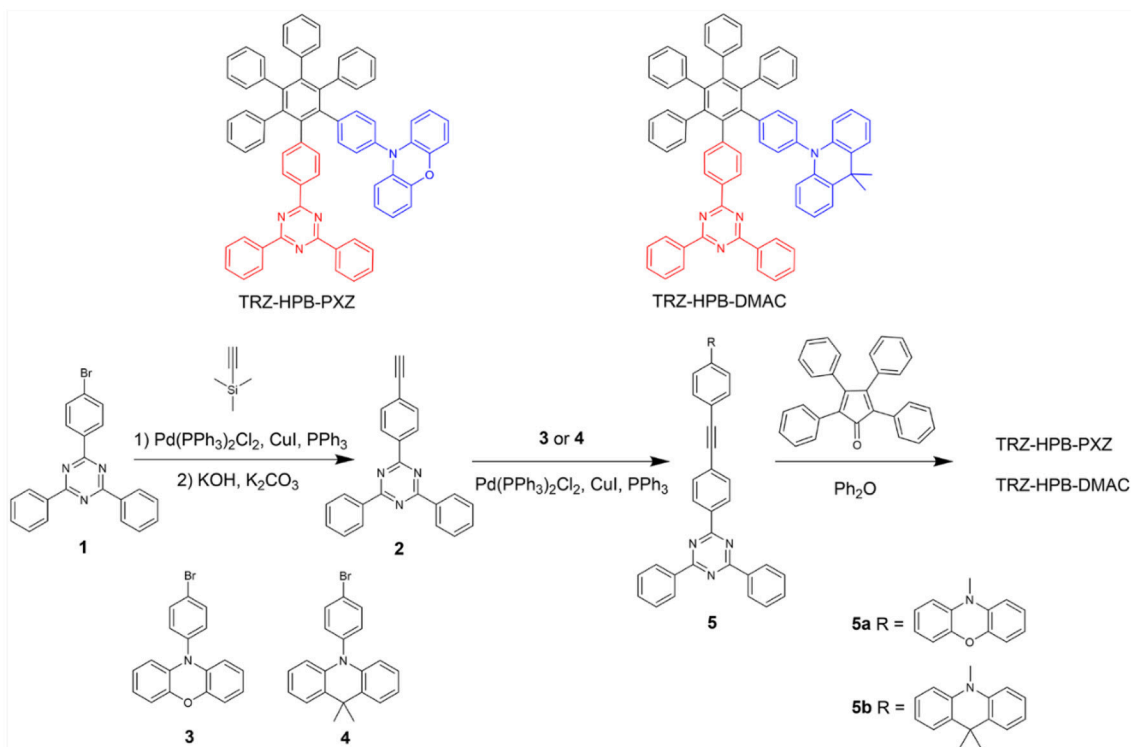
RESULTS AND DISCUSSION

The synthetic procedures of these new HPB-based molecules are described in **Scheme 1**. Intermediates **5a** and **5b** were prepared from compound **1** in two steps by Sonogashira reactions. Subsequently, the target TRZ-HPB-PXZ and TRZ-HPB-DMAC were synthesized through Diels-Alder reactions between **5a** and **5b** with tetraphenylcyclopentadienone, respectively. These HPB-based molecules were identified using ^1H NMR, ^{13}C NMR and high-resolution mass spectroscopy. The thermal stabilities of TRZ-HPB-PXZ and TRZ-HPB-DMAC were evaluated by differential scanning calorimetry (DSC) and thermogravimetric analysis (TGA) methods. They all exhibit good thermal

properties with high decomposition temperatures (T_d) of 450.4 and 464.9°C, respectively (**Figure 1A**). But no glass transition temperatures are observed. The results demonstrate that they are thermally stable and can be used as active layers in OLEDs by vacuum-deposition technique. The cyclic voltammetry was used to test their electrochemical behaviors. They have similar reversible oxidation and reduction processes (**Figure 1B**), indicative of good electrochemical stability. The

HOMO and LUMO energy levels are determined to be -5.02 and -2.68 eV for TRZ-HPB-PXZ, and -5.23 and -2.79 eV for TRZ-HPB-DMAC, respectively.

The single crystals of TRZ-HPB-DMAC were obtained from the THF-hexane mixture by slow solvent evaporation and subject to crystallography analysis. The crystal structure shows that the dihedral angles between 2,4,6-triphenyl-1,3,5-triazine (TRZ) and the central phenyl is 68.94° , and the dihedral



SCHEME 1 | Synthetic routes of TRZ-HPB-PXZ and TRZ-HPB-DMAC.

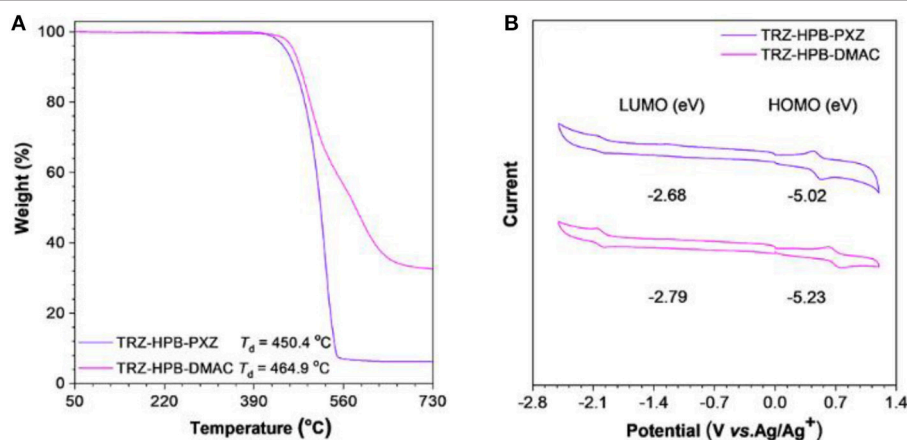


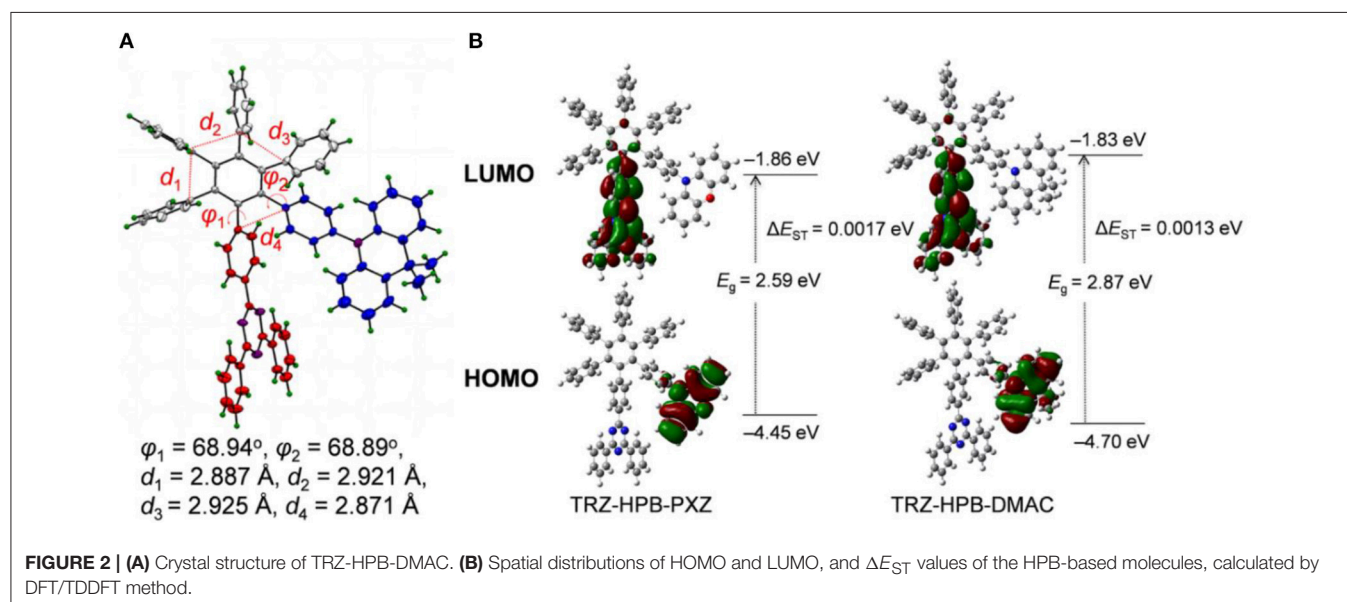
FIGURE 1 | **(A)** TGA curves of TRZ-HPB-PXZ and TRZ-HPB-DMAC, recorded under nitrogen at a heating rate of $20^\circ\text{C min}^{-1}$. **(B)** Cyclic voltammograms of TRZ-HPB-PXZ and TRZ-HPB-DMAC, measured in acetonitrile containing 0.1 M tetra-*n*-butylammonium hexafluorophosphate. Scan rate: 100 mV s^{-1} .

angles between 9,9-dimethyl-10-phenyl-acridine (DMAC) and the central phenyl is 68.89° , implying that through-bond conjugation is relatively weak. The six peripheral phenyl groups of HPB are connected to the central phenyl ring in a propeller-like fashion. They are closely aligned with the shortest distances <3.0 Å between adjacent phenyls (**Figure 2A**), indicating that there are strong electronic coupling interactions between these phenyl groups, namely through-space conjugation (Lambert, 2005; Zhen et al., 2018). Furthermore, the shortest distance between TRZ and DMAC is only 2.871 Å, which is close enough to produce intramolecular through-space electronic coupling, providing a charge transfer channel. The screwy architecture is of great importance to the separation of frontier orbitals, resulting in a small ΔE_{ST} . In addition, intermolecular C–H $\cdots\pi$ interactions are also observed (**Figure S1**), which are conducive to increasing the structural rigidity of the molecules and restraining intramolecular vibration that expedites non-radiative decay.

To gain insight into the molecular geometries and frontier orbital distributions, density functional theory (DFT) calculations were performed on these HPB-based molecules. The HOMO are mainly distributed on the electron-donating 10-phenyl-phenoxazine (PXZ) and DMAC moieties, while the LUMO are located on the electron-accepting TRZ moiety and partially extend to the central phenyl ring of HPB (**Figure 2B**). On one hand, the phenyls in HPB are aligned tightly in a highly twisted molecular conformation, resulting in the separation of HOMO and LUMO. On the other hand, the molecular orbitals are spatially proximate, allowing through-space charge transfer process to occur, and thus enhance the radiative decay rate. As a result, very small ΔE_{ST} and high PLQY can be expected, which make these materials promising candidates for efficient emitters. According to the time-dependent density functional theory (TD-DFT) calculations, the ΔE_{ST} values of TRZ-HPB-PXZ and TRZ-HPB-DMAC are estimated to be 0.0017 and 0.0013 eV, respectively, which are small enough for RISC process.

The absorption and PL spectra of these HPB-based molecules are depicted in **Figure 3**. There are distinct broad absorption shoulders in the range of 300–350 nm, which are associated with the intramolecular charge transfer (ICT), as confirmed by theoretical calculation (**Figure S2**). Their PL spectra in dilute THF solutions show two peaks. The weak PL bands at 370–390 nm are mainly attributable to the localized state emissions of donor and acceptor moieties (Kubota et al., 2014), while the strong PL peaks at 595 nm for TRZ-HPB-PXZ and 541 nm for TRZ-HPB-DMAC are assigned to the ICT state emissions of the molecules. Similar dual emissions have also been discovered by other research groups (Lee et al., 2015b; Shiu et al., 2017). The PL spectra display an apparent solvatochromic effect in different solvents (**Figure S3**). For example, the maximum PL peak of TRZ-HPB-PXZ shifts from 457 nm in hexane to 595 nm in THF. Analogous spectral movements are also found in TRZ-HPB-DMAC, indicative of their strong ICT characters. Both HPB-based molecules exhibit weak emissions in THF solutions with low PLQY of 5.5 and 9.1% (**Table 1**). However, their emissions are significantly enhanced when fabricated into neat films. The PL peak of TRZ-HPB-PXZ is located at around 576 nm and that of TRZ-HPB-DMAC is blue-shifted to 484 nm. High PLQY of 61.5 and 51.8% are recorded in neat films of TRZ-HPB-PXZ and TRZ-HPB-DMAC, respectively, which are improved by about one order of magnitude compared with those in solutions. The obvious increase in PLQY of TRZ-HPB-PXZ and TRZ-HPB-DMAC in neat films indicates that they should possess AIE character. To further corroborate the AIE nature of TRZ-HPB-PXZ and TRZ-HPB-DMAC, their PL spectra in THF/water mixtures were measured. It can be seen that along with the nanoaggregates formation by adding a large amount of water into THF solutions, the emissions of TRZ-HPB-PXZ and TRZ-HPB-DMAC are enhanced significantly (**Figure 3**), clearly validating the AIE nature (Mei et al., 2015).

To deepen the understanding of their PL properties, the transient PL decay spectra in THF/water mixtures and neat



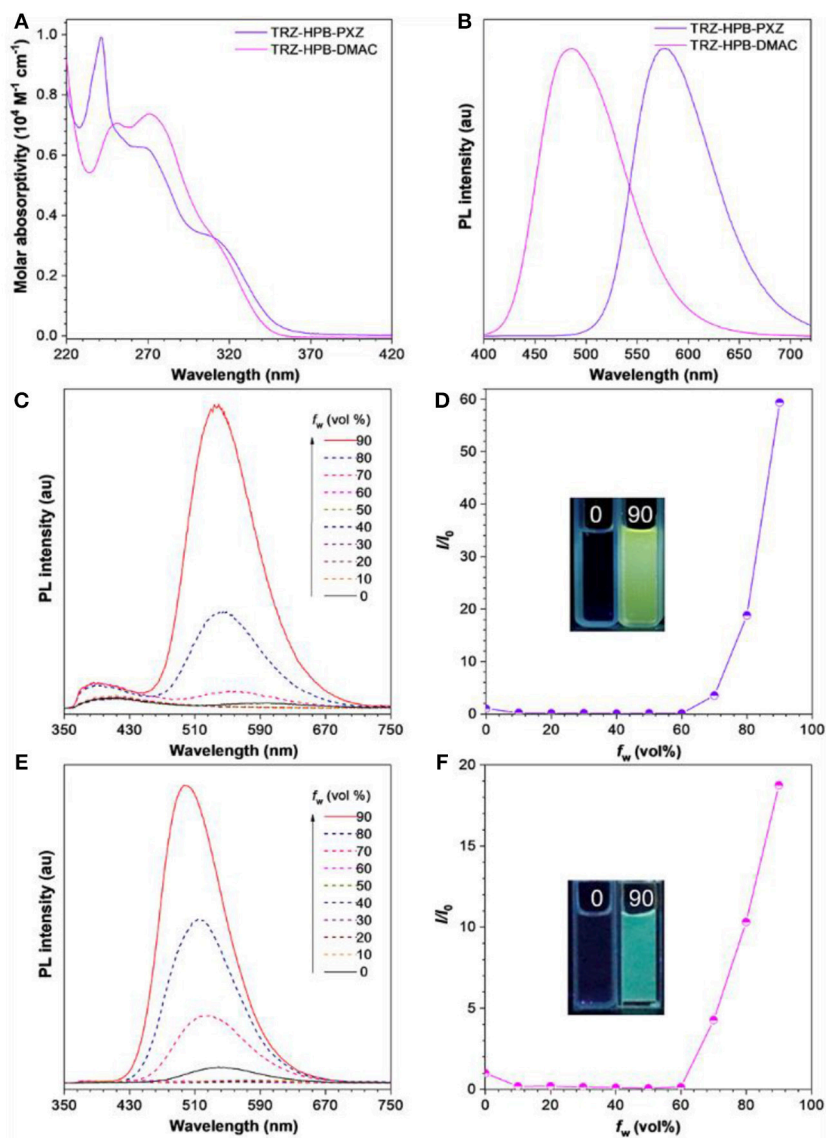


FIGURE 3 | (A) Absorption spectra of these HPB-based molecules in THF solutions (10^{-5} M). (B) PL spectra of these HPB-based molecules in neat films. PL spectra of (C) TRZ-HPB-PXZ, (E) TRZ-HPB-DMAC in THF/water mixtures with different water fractions (f_w), Plots of I/I_0 vs. f_w of (D) TRZ-HPB-PXZ, (F) TRZ-HPB-DMAC. I_0 is the PL intensity in pure THF. Inset: photographs of these HPB-based molecules in THF/water mixtures ($f_w = 0$ and 90%), taken under 310 nm excitation.

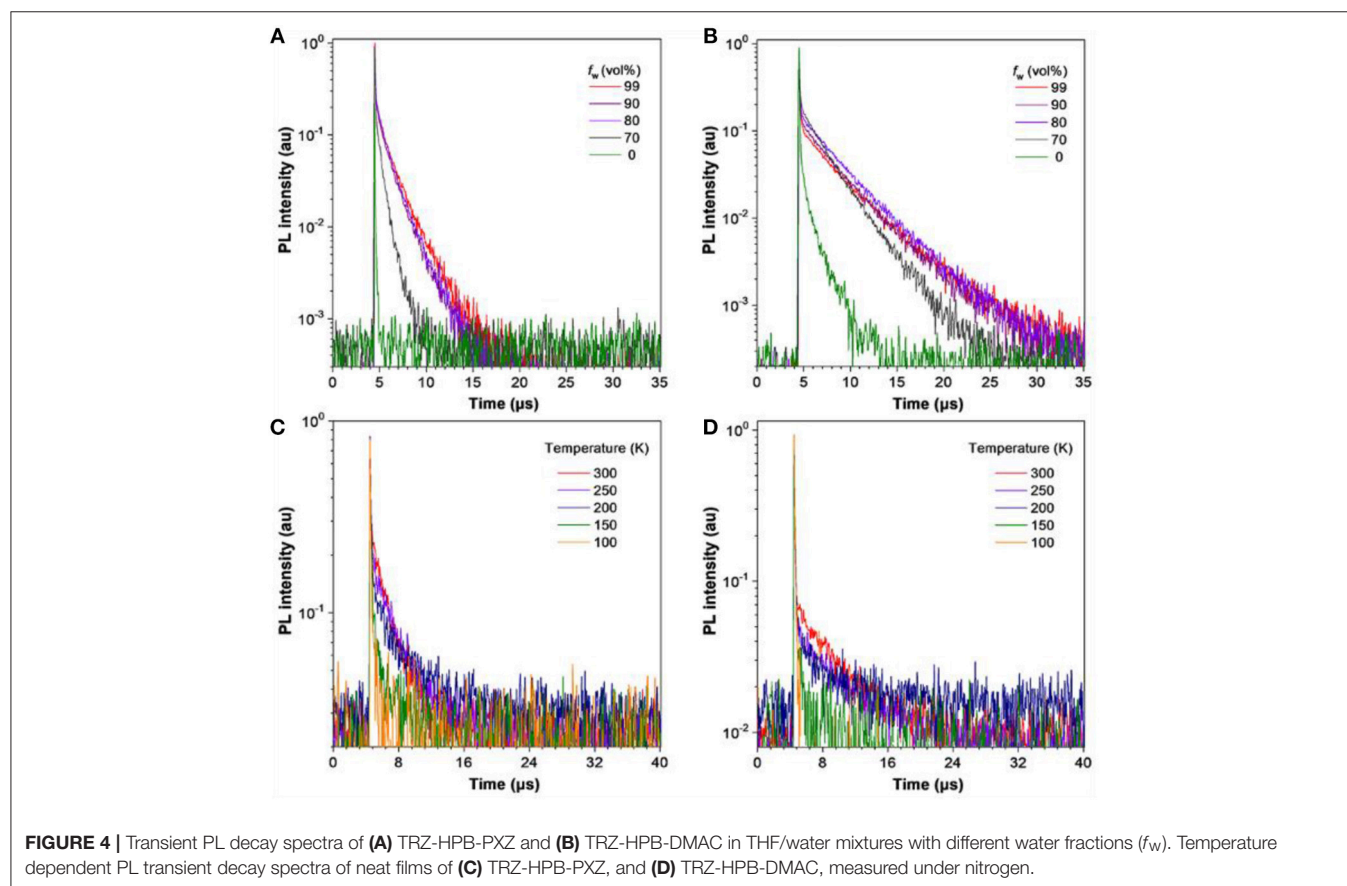
films were measured (Figure 4). Their PL decay profiles consist of two parts: a nanosecond-scale component and a microsecond-scale one, which can be attributed to prompt fluorescence and delayed fluorescence, respectively. In THF solution, TRZ-HPB-PXZ and TRZ-HPB-DMAC possess short mean lifetimes of 15.2 and 357.5 ns, respectively, and the delayed components are hardly recognizable (Table 1). However, prominent delayed components are discovered upon aggregate formation (Table S1), revealing that the delayed fluorescence is induced by aggregation (Aizawa et al., 2017; Gan et al., 2017; Guo et al., 2017a, 2018a; Huang et al., 2017; Liu et al., 2018). The neat films of TRZ-HPB-PXZ and TRZ-HPB-DMAC show long lifetimes in microsecond scale (1.8 and 3.4 μ s), which are significantly longer than those recorded in solutions

(Table S2), further demonstrating their AIDF attributes. When dispersed in good solvents, the intramolecular rotational, and vibrational motions are spiritedly active, and as a result, excited state energy is dissipated in a non-radiative manner via internal conversion (IC) (Li and Li, 2017), leading to faint emission. Besides, rapid IC process will impede intersystem crossing (ISC) and RISC processes, which is responsible for the indiscernible delayed fluorescence. Whereas, in aggregates, the molecular motions are restricted greatly because of the limited physical space, resulting in blocking of non-radiative IC channels and promotion of ISC and RISC processes under the basis of small ΔE_{ST} . Therefore, the molecules can emit strong emission with prominent delayed component (Fan et al., 2017; Guo et al., 2018b). The fluorescence decay is positively

TABLE 1 | Photophysical property of TRZ-HPB-PXZ and TRZ-HPB-DMAC.

	Solution ^a				Neat film ^b							
	λ_{abs} [nm]	λ_{em} [nm]	$\Phi_{\text{F}}^{\text{c}}$ [%]	$\langle\tau\rangle^{\text{d}}$ [ns]	λ_{em} [nm]	$\Phi_{\text{F}}^{\text{c}}$ [%]	$\langle\tau\rangle^{\text{d}}$ [ns]	$\tau_{\text{prompt}}^{\text{e}}$ [ns]	$\tau_{\text{delayed}}^{\text{e}}$ [μs]	R^{f} [%]	$k_{\text{RISC}}^{\text{g}}$ [$\times 10^5 \text{s}^{-1}$]	$\Delta E_{\text{ST}}^{\text{h}}$ [eV]
TRZ-HPB-PXZ	310	595	5.5	15.2	576	61.5	1798.4	41.6	2.1	84.8	31.0	0.02
TRZ-HPB-DMAC	310	541	9.1	357.5	484	51.8	3354.8	48.4	4.7	70.6	7.2	0.09

^aMeasured in THF solution (10^{-5} M) at room temperature. ^bVacuum-deposited on a quartz substrate. ^cDetermined by a calibrated integrating sphere under nitrogen at room temperature. ^dMean fluorescence lifetime evaluated at 300 K under nitrogen. ^eFluorescence lifetimes of prompt (τ_{prompt}) and delayed (τ_{delayed}) components evaluated at 300 K under nitrogen. ^fRatio of delayed component. ^gRate constant of RISC calculated from the equations given in the **Supplementary Material**. ^hEstimated from the high-energy onsets of fluorescence and phosphorescence spectra at 77 K.



correlated with temperature and the long-lived component is promoted as temperature increases (Table S3). The ΔE_{ST} values of these molecules were obtained from the singlet and triplet energies calculated from the onset of the fluorescence and phosphorescence spectra, respectively, measured in neat films at 77 K (Figure S4). TRZ-HPB-PXZ and TRZ-HPB-DMAC exhibit small ΔE_{ST} values of 0.02 and 0.09 eV coupled with fast RISC rate constants (k_{RISC}) of 3.1×10^6 and $7.2 \times 10^5 \text{ s}^{-1}$, respectively (Table S4), which are favorable for the occurrence of delayed fluorescence.

In view of excellent solid-state PL efficiencies, prominent delayed fluorescence as well as good thermal stability of

TRZ-HPB-PXZ and TRZ-HPB-DMAC, multilayer non-doped OLEDs were fabricated to investigate their EL properties. The configurations of devices were: ITO/HATCN (5 nm)/TAPC (20 nm)/TCTA (5 nm)/emitter/TmPyPB (55 nm)/LiF (1 nm)/Al, in which the neat films of TRZ-HPB-PXZ (35 nm) (device I) and TRZ-HPB-DMAC (20 nm) (device II) acted as emitters; dipyrzino[2,3-f:2',3'-h]quinoxaline-2,3,6,7,10,11-hexacarbonitrile (HATCN), 1,1'-bis(di-4-tolylaminophenyl)cyclohexane (TAPC), 1,3,5-tri(mpyrid-3-yl-phenyl)benzene (TmPyPB) and 4,4',4''-tris(carbazol-9-yl)-triphenylamine (TCTA) functioned as hole injection, hole-transporting, electron-transporting and

exciton-blocking layers, respectively. Appropriate adjustment of the emitter thickness had been made in order to achieve better device performance. The character curves are presented in **Figure 5** and the key data of the devices are listed in **Table 2**. Devices I and II are turned on at a low voltage of 2.5 and 3.1 V, respectively, implying efficient carrier injection and transport into the emitters. Device I emits bright yellow light ($\lambda_{\text{EL}} = 544 \text{ nm}$) with color coordinates of $\text{CIE}_{x,y}$ (0.39, 0.57). Its maxima current (η_{C}), power (η_{P}) and external quantum (η_{ext}) efficiencies are 41.2 cd A^{-1} , 44.9 lm W^{-1} , and 12.7%, respectively. More significantly, this non-doped device of TRZ-HPB-PXZ enjoys excellent efficiency stability. When the luminance is increased to $1,000 \text{ cd m}^{-2}$, the η_{C} , η_{P} , and η_{ext} still remain as 40.1 cd A^{-1} , 31.5 lm W^{-1} , and 12.3%, respectively. The roll-off of current efficiency is only 2.7%. The EL peak of device II is located at 521 nm ($\text{CIE}_{x,y} = 0.28, 0.58$) and the maximum η_{ext} is 6.5%. The

inferior EL performance may be due to the lower PLQY and increased ΔE_{ST} of TRZ-HPB-DMAC compared with those of TRZ-HPB-PXZ. It is noted that the EL spectra are shifted relative to their PL spectra in films. Similar differences are reported by other groups, which may be caused by optical microcavity effect or different excited dipole moments of the molecules under electrical excitation and photoexcitation (Chen et al., 2014; Sun et al., 2015; Zhang et al., 2016).

Theoretical maximum η_{ext} was also calculated in order to evaluate the exciton utilization of TRZ-HPB-PXZ-based device I. According to the values of entire PLQY and lifetime, the PLQY contributed by prompt fluorescence (Φ_{prompt}) and delayed fluorescence (Φ_{delayed}) of TRZ-HPB-PXZ neat film are 9.4 and 52.1% (**Table S4**), respectively. Assuming that the out-coupling efficiency is 20–30% and the charge transport is balanced, the maximum theoretical η_{ext} calculated from photophysical data of TRZ-HPB-PXZ is 12.3–18.5%

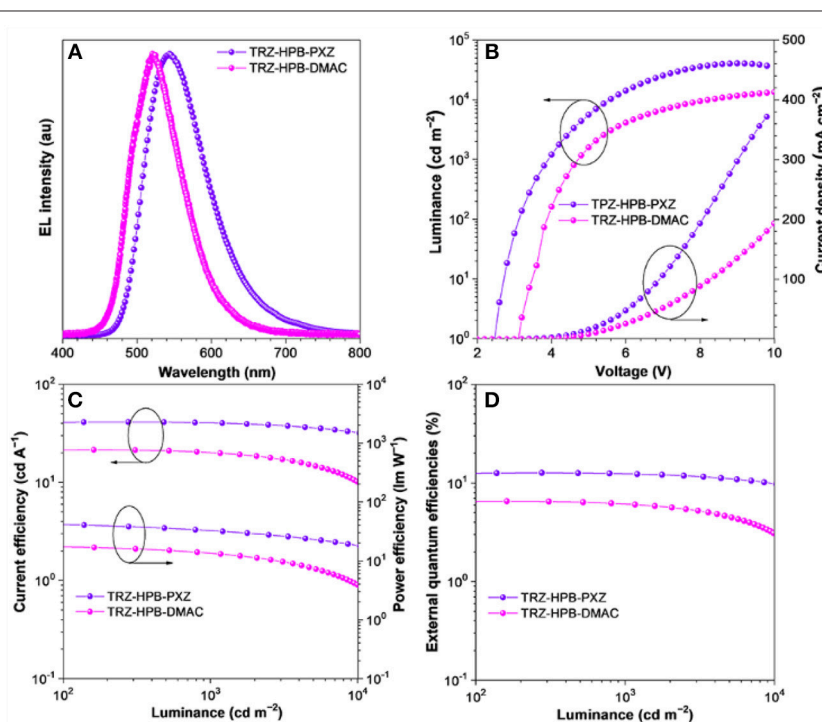


FIGURE 5 | (A) EL spectra at luminance of $1,000 \text{ cd m}^{-2}$, and characteristic curves of **(B)** luminance-voltage-current density, **(C)** current efficiency-luminance-power efficiency, and **(D)** external quantum efficiency-luminance of the non-doped OLEDs.

TABLE 2 | EL performances of the non-doped OLEDs based on HPB-based molecules^a.

Device	V_{on} [V]	Maximum values				Values at $1,000 \text{ cd m}^{-2}$						
		η_{C} [cd A^{-1}]	η_{P} [lm W^{-1}]	η_{ext} [%]	L [cd m^{-2}]	V [V]	η_{C} [cd A^{-1}]	η_{P} [lm W^{-1}]	η_{ext} [%]	RO [%]	λ_{EL} [nm]	CIE (x, y)
I	2.5	41.2	44.9	12.7	40,382	4.0	40.1	31.5	12.3	2.7	544	(0.39, 0.57)
II	3.1	21.4	17.6	6.5	15,460	4.8	19.9	13.0	6.0	7.0	521	(0.28, 0.58)

^a V_{on} , turn-on voltage at 1 cd m^{-2} ; η_{C} , current efficiency; η_{P} , power efficiency; η_{ext} , external quantum efficiency; L , luminance; CIE, Commission International de l'Eclairage coordinates; λ_{EL} , maxima of electroluminescent spectra; RO, current efficiency roll-off from maximum value to that at $1,000 \text{ cd m}^{-2}$. Emitter: TRZ-HPB-PXZ (device I); TRZ-HPB-DMAC (device II).

(Park et al., 2016), which is reasonable according to the experimental data, indicating that the triplet excitons have been sufficiently converted to radiative singlet excitons. However, the experimental η_{ext} of TRZ-HPB-DMAC is inferior to the maximum theoretical η_{ext} (10.3–15.5%). The phenomenon may be attributed to the poorer triplet-to-singlet conversion efficiency of TRZ-HPB-DMAC in EL devices due to the lower k_{RISC} , which is about one-fifth of TRZ-HPB-PXZ's k_{RISC} . In addition, the different carrier transport capabilities of PXZ and DMAC moieties will also influence the carrier balance in EL devices, and thus affect devices' performance. These results demonstrate that through-space charge transfer contributes to a small ΔE_{ST} and thus delayed fluorescence, which allows a high exciton utilization of the emitters. In addition, the intriguing AIDF properties are conducive to suppressing emission quenching and exciton annihilation in neat films. The synergistic effect of these factors ensures non-doped OLEDs with high efficiency and small efficiency roll-off.

CONCLUSIONS

In summary, two HPB-based luminogens TRZ-HPB-PXZ and TRZ-HPB-DMAC with good thermal and electrochemical stabilities are synthesized and characterized. Both luminogens exhibit through-space charge transfer feature between D and A moieties, which brings about efficient separation of HOMO and LUMO, and thus small ΔE_{ST} . TRZ-HPB-PXZ and TRZ-HPB-DMAC are barely fluorescent in solutions but show strong emissions with prominent delayed fluorescence in the aggregated state, that is AIDF property. Their neat films have distinct delayed fluorescence and high PLQY. Non-doped

OLEDs using these luminogens as light-emitting layers have achieved excellent performance with a maximum η_{ext} of 12.7% and very small efficiency roll-off of 2.7% at 1,000 cd m⁻². These results reveal that AIDF luminogens with through-space charge transfer can realize high exciton utilization and suppressed exciton annihilation at high luminance, which could be promising candidates for OLEDs with improved efficiency and stability.

AUTHOR CONTRIBUTIONS

All authors listed have made a substantial, direct and intellectual contribution to the work, and approved it for publication.

ACKNOWLEDGMENTS

This study was financially supported by the National Natural Science Foundation of China (21788102 and 21673082), the National Basic Research Program of China (973 Program, 2015CB655004) Funded by MOST, the Guangdong Natural Science Funds for Distinguished Young Scholar (2014A030306035), the Natural Science Foundation of Guangdong Province (2016A030312002 and 2016B090907001), the Science and Technology Program of Guangzhou (201804020027 and 201704030069) and the Innovation and Technology Commission of Hong Kong (ITC-CNERC14SC01).

SUPPLEMENTARY MATERIAL

The Supplementary Material for this article can be found online at: <https://www.frontiersin.org/articles/10.3389/fchem.2019.00199/full#supplementary-material>

REFERENCES

- Adachi, C., Baldo, M. A., Thompson, M. E., and Forrest, S. R. (2001). Nearly 100% internal phosphorescence efficiency in an organic light-emitting device. *J. Appl. Phys.* 90:5048. doi: 10.1063/1.1409582
- Aizawa, N., Tsou, C.-J., Park, I. S., and Yasuda, T. (2017). Aggregation-induced delayed fluorescence from phenothiazine-containing donor-acceptor molecules for high-efficiency non-doped organic light-emitting diodes. *Polym. J.* 49, 197–202. doi: 10.1038/pj.2016.82
- Baldo, M. A., O'Brien, D. F., You, Y., Shoustikov, A., Sibley, S., Thompson, M. E., et al. (1998). Highly efficient phosphorescent emission from organic electroluminescent devices. *Nature* 395, 151–154. doi: 10.1038/25954
- Balzani, V., Clemente-León, M., Credi, A., Lowe, J. N., Badjić, J. D., Stoddart, J. F., et al. (2003). Controlling multivalent interactions in triply-threaded two-component superbundles. *Chem. Eur. J.* 9, 5348–5360. doi: 10.1002/chem.200304979
- Cao, X., Zhang, D., Zhang, S., Tao, Y., and Huang, W. (2017). CN-Containing donor-acceptor-type small-molecule materials for thermally activated delayed fluorescence OLEDs. *J. Mater. Chem. C* 5, 7699–7714. doi: 10.1039/c7tc02481a
- Chen, L., Jiang, Y., Nie, H., Hu, R., Kwok, H. S., Huang, F., et al. (2014). Rational design of aggregation-induced emission luminogen with weak electron donor-acceptor interaction to achieve highly efficient undoped bilayer OLEDs. *ACS Appl. Mater. Interfaces* 6, 17215–17225. doi: 10.1021/am505036a
- Chen, X. L., Jia, J. H., Yu, R., Liao, J. Z., Yang, M. X., and Lu, C. Z. (2017). Combining charge-transfer pathways to achieve unique thermally activated delayed fluorescence emitters for high-performance solution-processed, non-doped blue OLEDs. *Angew. Chem. Int. Ed.* 56, 15006–15009. doi: 10.1002/anie.201709125
- Cho, S., Li, W. S., Yoon, M. C., Ahn, T. K., Jiang, D. L., Kim, J., et al. (2006). Relationship between incoherent excitation energy migration processes and molecular structures in Zinc (II) porphyrin dendrimers. *Chem. Eur. J.* 12, 7576–7584. doi: 10.1002/chem.200600213
- Endo, A., Ogasawara, M., Takahashi, A., Yokoyama, D., Kato, Y., and Adachi, C. (2009). Thermally activated delayed fluorescence from Sn⁴⁺-porphyrin complexes and their application to organic light emitting diodes—A novel mechanism for electroluminescence. *Adv. Mater. Weinheim.* 21, 4802–4806. doi: 10.1002/adma.200900983
- Fan, J., Lin, L., and Wang, C.-K. (2017). Excited state properties of non-doped thermally activated delayed fluorescence emitters with aggregation-induced emission: a QM/MM study. *J. Mater. Chem. C* 5, 8390–8399. doi: 10.1039/c7tc02541f
- Furue, R., Nishimoto, T., Park, I. S., Lee, J., and Yasuda, T. (2016). Aggregation-induced delayed fluorescence based on donor/acceptor-tethered janus carborane triads: unique photophysical properties of non-doped OLEDs. *Angew. Chem. Int. Ed.* 55, 7171–7175. doi: 10.1002/anie.201603232
- Gan, S., Luo, W., He, B., Chen, L., Nie, H., Hu, R., et al. (2016). Integration of aggregation-induced emission and delayed fluorescence into electronic donor-acceptor conjugates. *J. Mater. Chem. C* 4, 3705–3708. doi: 10.1039/c5tc03588k

- Gan, S., Zhou, J., Smith, T. A., Su, H., Luo, W., Hong, Y., et al. (2017). New AIEgens with delayed fluorescence for fluorescence imaging and fluorescence lifetime imaging of living cells. *Mater. Chem. Front.* 1, 2554–2558. doi: 10.1039/c7qm00286f
- Geng, Y., Fechtenkötter, A., and Müllen, K. (2001). Star-like substituted hexaarylbenzenes: synthesis and mesomorphic properties. *J. Mater. Chem.* 11, 1634–1641. doi: 10.1039/b101163o
- Gong, S., Chen, Y., Luo, J., Yang, C., Zhong, C., Qin, J., et al. (2011). Bipolar tetraarylsilanes as universal hosts for blue, green, orange, and white electrophosphorescence with high efficiency and low efficiency roll-off. *Adv. Funct. Mater.* 21, 1168–1178. doi: 10.1002/adfm.201002066
- Guo, J., Fan, J., Lin, L., Zeng, J., Liu, H., Wang, C. K., et al. (2018b). Mechanical insights into aggregation-induced delayed fluorescence materials with anti-kasha behavior. *Adv. Sci.* 6:1801629. doi: 10.1002/advs.201801629
- Guo, J., Li, X.-L., Nie, H., Luo, W., Gan, S., Hu, S., et al. (2017a). Achieving high-performance non-doped OLEDs with extremely small efficiency roll-off by combining aggregation-induced emission and thermally activated delayed fluorescence. *Adv. Funct. Mater.* 27:1606458. doi: 10.1002/adfm.201606458
- Guo, J., Li, X.-L., Nie, H., Luo, W., Hu, R., Qin, A., et al. (2017b). Robust luminescent materials with prominent aggregation-induced emission and thermally activated delayed fluorescence for high-performance organic light-emitting diodes. *Chem. Mater.* 29, 3623–3631. doi: 10.1021/acs.chemmater.7b00450
- Guo, J., Zhao, Z., and Tang, B. Z. (2018a). Purely organic materials with aggregation-induced delayed fluorescence for efficient nondoped OLEDs. *Opt. Mater.* 6:1800264. doi: 10.1002/adom.201800264
- Hirata, S., Sakai, Y., Masui, K., Tanaka, H., Lee, S. Y., Nomura, H., et al. (2015). Highly efficient blue electroluminescence based on thermally activated delayed fluorescence. *Nat. Mater.* 14, 330–336. doi: 10.1038/nmat4154
- Huang, J., Nie, H., Zeng, J., Zhuang, Z., Gan, S., Cai, Y., et al. (2017). Highly efficient non-doped OLEDs with negligible efficiency roll-off fabricated from aggregation-induced delayed fluorescence luminogens. *Angew. Chem. Int. Ed.* 56, 12971–12976. doi: 10.1002/anie.201706752
- Kaji, H., Suzuki, H., Fukushima, T., Shizu, K., Suzuki, K., Kubo, S., et al. (2015). Purely organic electroluminescent material realizing 100% conversion from electricity to light. *Nat. Commun.* 6:8476. doi: 10.1038/ncomms9476
- Kanibolotsky, A. L., Perepichka, I. F., and Skabara, P. J. (2010). Star-shaped π -conjugated oligomers and their applications in organic electronics and photonics. *Chem. Soc. Rev.* 39, 2695–2728. doi: 10.1039/b918154g
- Kawsumi, K., Wu, T., Zhu, T., Chae, H. S., Van Voorhis, T., Baldo, M. A., et al. (2015). Thermally activated delayed fluorescence materials based on homoconjugation effect of donor-acceptor triptycenes. *J. Am. Chem. Soc.* 137, 11908–11911. doi: 10.1021/jacs.5b07932
- Kubota, Y., Sakuma, Y., Funabiki, K., and Matsui, M. (2014). Solvatochromic fluorescence properties of pyrazine-boron complex bearing a β -Iminoenolate ligand. *J. Phys. Chem. A* 118, 8717–8729. doi: 10.1021/jp506680g
- Lambert, C. (2005). Hexaarylbenzenes—prospects for toroidal delocalization of charge and energy. *Angew. Chem. Int. Ed.* 44, 7337–7339. doi: 10.1002/anie.200502105
- Lambert, C., Ehbets, J., Rausch, D., and Steeger, M. (2012). Charge-transfer interactions in a multichromophoric hexaarylbenzene containing pyrene and triarylamines. *J. Org. Chem.* 77, 6147–6154. doi: 10.1021/jo300924x
- Lee, D. R., Kim, B. S., Lee, C. W., Im, Y., Yook, K. S., Hwang, S.-H., et al. (2015a). Above 30% external quantum efficiency in green delayed fluorescent organic light-emitting diodes. *ACS Appl. Mater. Interfaces* 7, 9625–9629. doi: 10.1021/acsami.5b01220
- Lee, J., Shizu, K., Tanaka, H., Nakanotani, H., Yasuda, T., Kaji, H., et al. (2015b). Controlled emission colors and singlet-triplet energy gaps of dihydrophenazine-based thermally activated delayed fluorescence emitters. *J. Mater. Chem. C* 3, 2175–2181. doi: 10.1039/c4tc02530j
- Li, Q., and Li, Z. (2017). The strong light-emission materials in the aggregated state: what happens from a single molecule to the collective group. *Adv. Sci.* 4:1600484. doi: 10.1002/advs.201600484
- Liu, H., Zeng, J., Guo, J., Nie, H., Zhao, Z., and Tang, B. Z. (2018). High-performance non-doped OLEDs with nearly 100 % exciton use and negligible efficiency roll-off. *Angew. Chem. Int. Ed.* 130, 9434–9438. doi: 10.1002/ange.201802060
- Mei, J., Leung, N. L. C., Kwok, R. T. K., Lam, J. W. Y., and Tang, B. Z. (2015). Aggregation-induced emission: together we shine, united we soar! *Chem. Rev.* 115, 11718–11940. doi: 10.1021/acs.chemrev.5b00263
- Minaev, B., Baryshnikov, G., and Agren, H. (2014). Principles of phosphorescent organic light emitting devices. *Phys. Chem. Chem. Phys.* 16, 1719–1758. doi: 10.1039/c3cp53806k
- Park, I. S., Lee, S. Y., Adachi, C., and Yasuda, T. (2016). Full-color delayed fluorescence materials based on wedge-shaped phthalonitriles and dicyanopyrazines: systematic design, tunable photophysical properties, and OLED performance. *Adv. Funct. Mater.* 26, 1813–1821. doi: 10.1002/adfm.201505106
- Rajamalli, P., Senthilkumar, N., Gandeepan, P., Huang, P. Y., Huang, M. J., Ren-Wu, C. Z., et al. (2016). A new molecular design based on thermally activated delayed fluorescence for highly efficient organic light emitting diodes. *J. Am. Chem. Soc.* 138, 628–634. doi: 10.1021/jacs.5b10950
- Sasabe, H., and Kido, J. (2013). Recent progress in phosphorescent organic light-emitting devices. *Eur. J. Org. Chem.* 2013, 7653–7663. doi: 10.1002/ejoc.201300544
- Seino, Y., Inomata, S., Sasabe, H., Pu, Y. J., and Kido, J. (2016). High-performance green OLEDs using thermally activated delayed fluorescence with a power efficiency of over 100 lm W⁻¹. *Adv. Mater. Weinheim.* 28, 2638–2643. doi: 10.1002/adma.201503782
- Shao, S., Hu, J., Wang, X., Wang, L., Jing, X., and Wang, F. (2017). Blue thermally activated delayed fluorescence polymers with non-conjugated backbone and through-space charge transfer effect. *J. Am. Chem. Soc.* 139, 17739–17742. doi: 10.1021/jacs.7b10257
- Shiu, Y.-J., Chen, Y.-T., Lee, W.-K., Wu, C.-C., Lin, T.-C., Liu, S.-H., et al. (2017). Efficient thermally activated delayed fluorescence of functional phenylpyridinato boron complexes and high performance organic light-emitting diodes. *J. Mater. Chem. C* 5, 1452–1462. doi: 10.1039/c6tc04994j
- Sun, D., Rosokha, S. V., and Kochi, J. K. (2005). Through-space (cofacial) π -delocalization among multiple aromatic centers: toroidal conjugation in hexaphenylbenzene-like radical cations. *Angew. Chem. Int. Ed.* 44, 5133–5136. doi: 10.1002/anie.200501005
- Sun, J. W., Baek, J. Y., Kim, K.-H., Moon, C.-K., Lee, J.-H., Kwon, S.-K., et al. (2015). Thermally activated delayed fluorescence from azasilene based intramolecular charge-transfer emitter (DTPDDA) and a highly efficient blue light emitting diode. *Chem. Mater.* 27, 6675–6681. doi: 10.1021/acs.chemmater.5b02515
- Sun, J. W., Lee, J.-H., Moon, C.-K., Kim, K.-H., Shin, H., and Kim, J.-J. (2014). A fluorescent organic light-emitting diode with 30% external quantum efficiency. *Adv. Mater. Weinheim.* 26, 5684–5688. doi: 10.1002/adma.201401407
- Tanaka, Y., Koike, T., and Akita, M. (2010). 2-Dimensional molecular wiring based on toroidal delocalization of hexaarylbenzene. *Chem. Commun.* 46, 4529–4531. doi: 10.1039/c0cc00128g
- Tang, C. W., and VanSlyke, S. A. (1987). Organic electroluminescent diodes. *Appl. Phys. Lett.* 51:913. doi: 10.1063/1.98799
- Tao, Y., Yuan, K., Chen, T., Xu, P., Li, H., Chen, R., et al. (2014). Thermally activated delayed fluorescence materials towards the breakthrough of organoelectronics. *Adv. Mater. Weinheim.* 26, 7931–7958. doi: 10.1002/adma.201402532
- Tsujimoto, H., Ha, D. G., Markopoulos, G., Chae, H. S., Baldo, M. A., and Swager, T. M. (2017). Thermally activated delayed fluorescence and aggregation induced emission with through-space charge transfer. *J. Am. Chem. Soc.* 139, 4894–4900. doi: 10.1021/jacs.7b00873
- Vij, V., Bhalla, V., and Kumar, M. (2016). Hexaarylbenzene: evolution of properties and applications of multitiered scaffold. *Chem. Rev.* 116, 9565–9627. doi: 10.1021/acs.chemrev.6b00144
- Waldvogel, S. R., Wartini, A. R., and Rasmussen, P. H. Jr. (1999). A triphenylene scaffold with C_{3v}-symmetry and nanoscale dimensions. *Tetrahedron Lett.* 40, 3515–3518. doi: 10.1016/s0040-4039(99)00545-6
- Wang, H., Xie, L., Peng, Q., Meng, L., Wang, Y., Yi, Y., et al. (2014). Novel thermally activated delayed fluorescence materials-thioxanthone derivatives and their applications for highly efficient OLEDs. *Adv. Mater. Weinheim.* 26, 5198–5204. doi: 10.1002/adma.201401393

- Zhang, J., Ding, D., Wei, Y., and Xu, H. (2016). Extremely condensing triplet states of DPEPO-type hosts through constitutional isomerization for high-efficiency deep-blue thermally activated delayed fluorescence diodes. *Chem. Sci.* 7, 2870–2882. doi: 10.1039/c5sc04848f.
- Zhang, Q., Li, B., Huang, S., Nomura, H., Tanaka, H., and Adachi, C. (2014). Efficient blue organic light-emitting diodes employing thermally activated delayed fluorescence. *Nat. Photonics* 8, 326–332. doi: 10.1038/nphoton.2014.12
- Zhen, S., Mao, J. C., Chen, L., Ding, S., Luo, W., Zhou, X. S., et al. (2018). Remarkable multichannel conductance of novel single-molecule wires built on through-space conjugated hexaphenylbenzene. *Nano Lett.* 18, 4200–4205. doi: 10.1021/acs.nanolett.8b01082

Conflict of Interest Statement: The authors declare that the research was conducted in the absence of any commercial or financial relationships that could be construed as a potential conflict of interest.

Copyright © 2019 Zhang, Zeng, Guo, Zhen, Xiao, Wang, Zhao and Tang. This is an open-access article distributed under the terms of the Creative Commons Attribution License (CC BY). The use, distribution or reproduction in other forums is permitted, provided the original author(s) and the copyright owner(s) are credited and that the original publication in this journal is cited, in accordance with accepted academic practice. No use, distribution or reproduction is permitted which does not comply with these terms.